Proceedings of the ASME 2021 40th International Conference on Ocean, Offshore and Arctic Engineering
OMAE2021
June 21-30, 2021, Virtual, Online

OMAE2021-63738

2D NUMERICAL STUDY ON WAKE SCENARIOS FOR A FLAPPING FOIL

Hui-li Xu
Marine Technology Dept., NTNU
Trondheim, Norway

Marilena Greco
Marine Technology Dept., NTNU
Trondheim, Norway
CNR-INM, Inst. of Marine Eng.,
Rome, Italy

Claudio Lugni
Marine Technology Dept., NTNU
Trondheim, Norway
CNR-INM, Inst. of Marine Eng.,
Rome, Italy

ABSTRACT

Fishes are talented swimmers. Depending on the propulsion mechanisms many fishes can use flapping tails and/or fins to generate thrust, which seems to be connected to the formation of a reverse von Kármán wake. In the present work, the flow past a 2D flapping foil is simulated by solving the incompressible Navier-Stokes equations in the open-source OpenFOAM platform. A systematic study by varying the oscillating frequency, peak-to-peak amplitude and Reynolds number has been performed to analyze the transition of vorticity types in the wake as well as drag-thrust transition. The overset grid method is used herein to allow the pitching foil to move without restrictions. Spatial convergence tests have been carried out with respect to grid resolution and the size of overset mesh domain. Numerical results are compared with available experimental data and discussed. The results show that the adopted methodology can be well applied to simulate large amplitude motions of the flapping foil. The transitions in the types of wake are consistent with the benchmark experimental data, and the drag-thrust transition of the pitching foil does not coincide with von Kármán (vK)-reverse von Kármán (reverse-vK) wake transition and it is highly dependent on the Reynolds number.

Keywords: CFD, Flapping foil, Numerical features, Vortex shedding, Drag–thrust transition

NOMENCLATURE

A	peak-to-peak amplitude of forced oscillations
c	foil chord length
D	foil thickness
f	frequency of forced oscillations
L	fish length
T	foil oscillation period
U	uniform inflow velocity
ρ	density of fluid
ν	kinematic viscosity of fluid
θ	pitching angle of foil
A_D	amplitude-to-foil thickness ratio $A_D = A/D$
Sr	thickness based Strouhal number $Sr = fD/U$
Sr_A	amplitude based Strouhal number $= fA/U$
Re_c	chord based Reynolds number $= Uc/\nu$
Re_L	length based Reynolds number $= UL/\nu$

1. INTRODUCTION

Many aquatic animals can be considered as highly performant underwater bio vehicles with high hydrodynamic efficiency. The Strouhal number, defined as the product of the flapping frequency and characteristic wake width divided by the advancing speed, is employed to characterize the features of fish generated wake and so the fish thrust. Laboratory and theoretical studies suggest the optimal propulsive performance incurred by a flapping foil is within a narrow interval $0.2 < Sr_A < 0.4$ [1], which is consistent with the range adopted by many aquatic animals regardless of the sizes and species [2]. It confirms that these native swimmers have been evolved to cruise at an optimal strategy to minimize the energy cost during natural selection. Thus, many studies have focused on the analysis and implementation of transferring these biological configurations into biomimetic marine designs [3]. The majority of these aquatic animals generate thrust through the oscillating motion of their foil-like body and/or fins. This propulsion mechanism seems to be connected with formation of a reverse von Kármán wake, wherein the shed vortices induce a velocity in the same direction as the mean flow and create a velocity excess [4]. Therefore, it is essential to investigate vortices in the wake for a better understanding of this form of propulsion with the objective of creating innovative solutions for greener and efficient marine transportation. In addition, a free-swimming fish operates as a self-propelled vehicle, i.e., its thrust equals its experienced drag, which leads to a dilemma about identifying them individually.

Flapping foils can lead to the formation of various vortex patterns [5], and observation into the vortex processes is vital for understanding how an oscillating foil generates propulsive

forces. These different wake scenarios include, for example, von Kármán (vK) vortex street in which two vortices of opposite sign are shed per oscillatory period (2S) and wakes where two vortex pairs are shed per oscillation period (2P) [6]. There has been extensive work on flow visualizations pertaining to foils. In the study of Godoy-Diana et al. [7], the vK-type wakes and the reverse-vK wakes behind a pitching hydrofoil were measured using particle image velocimetry (PIV) techniques. The vK / reverse-vK wake transition is considered to occur when the vortices align along the symmetry line of the wake. The reversed-vK wake plays a significant role in biological locomotion [8]. Besides, other complex wakes such as 2P can also be important for swimming of aquatic animals [9]. Schnipper et al. [10] used a gravity-driven vertically flowing soap film to visualize a variety of wakes behind a pitching foil with up to 16 vortices per oscillation period, including vK vortex street, inverted-vK vortex street, 2P wake, 2P+2S wake and novel wakes ranging from 4P to 8P, as shown in Fig. 1. The wake types are mapped out in a phase diagram spanned by the thickness based Strouhal number and the dimensionless flapping amplitude. This allows us to investigate the significant wake transition from vK to the reverse-vK by increasing flapping frequency and/or amplitude.

The hydrodynamic forces acting on the flapping foil depend on the vortex formation and on the consequent features of the fluid-structure interactions; identifying these links are essential in order to understand the propulsion mechanisms. Many researchers have performed systemic work with respect to the force generation and wake structures of a flapping foil. From the comparison of wake-scenarios phase diagram and measured forces, it is found that the wake transition from vK to reverse-vK vortex street is not exactly consistent with the force transition from drag to thrust [7, 10]. In the classical inviscid theory, a flapping foil is expected to experience a thrust force when it produces the reverse vK wake, and the boundary between the vK / reverse-vK wake scenarios is also treated as the force transition boundary from drag to thrust.

Numerous recent studies have provided a wealth of data in terms of flapping motions and wake flow field at different Reynolds numbers. Experimental data for flapping hydrofoils suggest that fish prefer to swim near a 'universal' optimal Strouhal number because the propulsive efficiency (defined to be the ratio of useful power over input power, $\eta_P = FU/P$) is maximized there [8]. However, it is shown for carangiform swimmers that the optimal Strouhal number depends strongly on the swimming speed and, more precisely, by the involved fish length (L) based Reynolds number $Re_L = UL/\nu$ [11]. In the work of Chao et al. [12], the drag–thrust transition of a pitching foil with various chord lengths was studied to find the link between Sr_A and the chord-based Reynolds number, Re_c. However, the foil shape was changed together with Re_c and this effect on the force transition was not well discussed. In the present numerical simulations, a systematic investigation of flapping foils over a range of Re_c and Sr_A is performed by varying kinematic viscosities to reveal the dependence of the drag-thrust transition on Re_c.

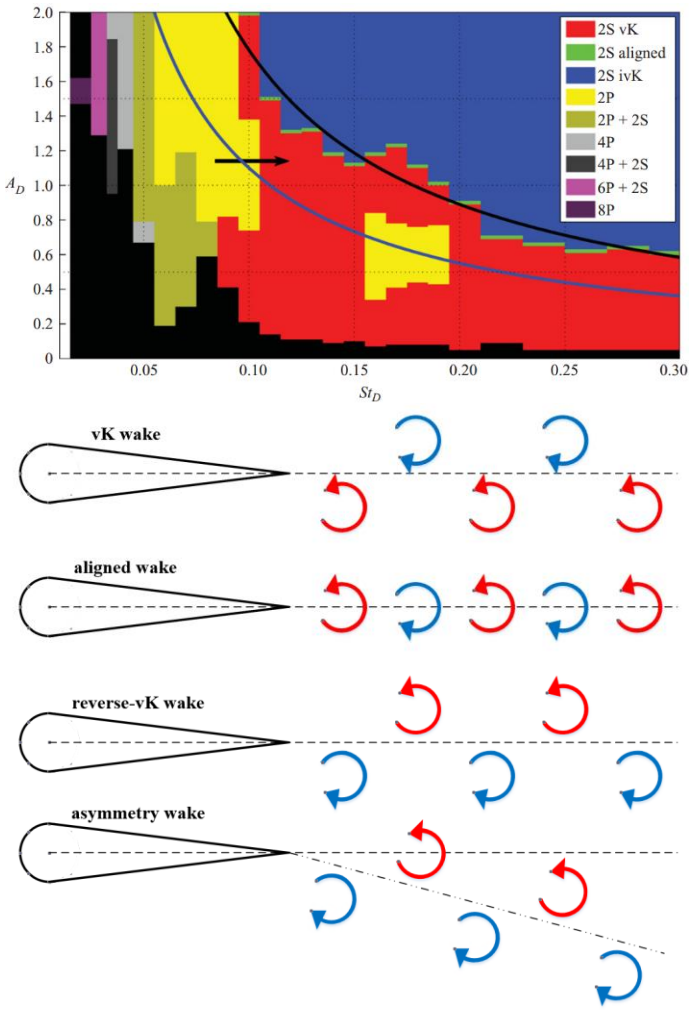

FIGURE 1: TOP: PHASE DIAGRAM OF VORTEX SYNCHRONIZATION REGIONS, FROM SCHNIPPER ET AL. [10] BOTTOM: SCHEMATIC VIEW OF SOME TYPICAL TYPES OF WAKE STRUCTURES.

With ever increasing computational power, CFD models have become more popular in the field of hydrodynamic studies. Extensive studies have been carried out for predicting the flow past flapping foils in the last few years [13]. Commercial software is relevant for use in industrial applications but can be inconvenient to modify for specific user requirements. Therefore, open-source CFD solvers like OpenFOAM are attractive, especially within the research community. These solvers are particularly advantageous due to the availability of large number and type of utilities for pre-processing, solution and post-processing of CFD problems. In addition, easy implementation of user-defined routines makes them very valuable for developers and researchers. This paper adopts OpenFOAM to simulate the flow past a flapping foil in a freestream.

This paper is organized as follows. First, we present the details of the flapping foil model, prescribed kinematics and the

employed numerical method in brief. The proposed method is validated against available experimental data. We then discuss the numerical experiments and the results in terms of wake scenarios, drag-thrust transition, and the influence of Reynolds number on the force transition. Lastly the conclusions of this work are provided.

2. MODELLING AND METHODOLOGY

2.1 Parameters of the flapping foil

The numerical study is based on the pitching foil experiments in a hydrodynamic tunnel by Godoy-Diana et al. [7], used here as reference data. A rigid symmetric foil is modelled with a semicircular leading edge and a triangular section in the aft, as shown in Fig. 2. The foil is placed in the uniform current with constant flow speed U in the horizontal direction parallel to the x-axis.

The flapping hydrofoil is forced to perform pitching motions (about O and z-axis) and the angular motions are described by:

$$\theta(t) = \theta_0 sin(\omega t) \quad (1)$$

where ω is the angular frequency, and θ_0 is the maximum pitching angle.

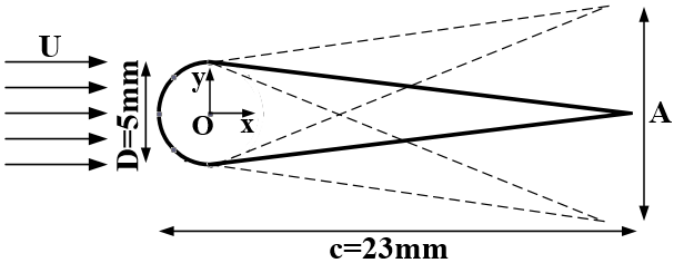

FIGURE 2: SCHEMATIC VIEW OF THE FOIL PROFILE AND PARAMETERS DEFINITION

The Reynolds number is based on foil chord length $Re_c = Uc/\nu$, where c is the foil chord length and ν is the kinematic viscosity of fluid. Its value was 1173 in the reference experiments [7]. Other important parameters are the nondimensional flapping amplitude and a sort of Strouhal number defined by Godoy-Diana et al. [7], respectively, as $A_D = A/D$ and $Sr = fD/U$, with f the foil forced-oscillation frequency and A the prescribed peak-to-peak amplitude.

2.1 Solution strategy

The flow past a flapping foil is in general a rotational-flow problem but viscosity also directly matters since an inviscid theory does not identify exactly the drag-thrust transition, depending on the Reynolds number. The open-source OpenFOAM platform is used in the present work with the assumption of viscous flow, without turbulence-flow model and in two-dimensional (2D) conditions. The 2D simulation is made consistently with the reference experimental study which supports a quasi-2D mechanism. The resulting model corresponds to a direct numerical simulation (DNS) if the used discretization can capture the physics of the problem. For the examined foil case, the flow is laminar close to the body while transition to turbulence can happen in the far field. In this context, one should note that turbulence leads, in a real environment, to three-dimensional (3D) features. It means that, even though we were able to capture the small scale of the turbulence in the far field, we would not be able to capture its evolution in proper way (direct cascade in 3D, inverse in 2D), and including a turbulent-flow model within a 2D-flow assumption would not lead to an improvement. The comparison against the experiments (in terms of local and global quantities) can help in quantifying the importance of this possible error source in the numerical model. OpenFOAM employs a finite volume discretization (FVD) technique on a collocated grid in the fluid domain. The numerical method employed for solving the incompressible Navier-Stokes equation is the PIMPLE algorithm, which is a combination of PISO (Pressure Implicit with Splitting of Operator) and SIMPLE (Semi-Implicit Method for Pressure Linked Equations) algorithms. A second order scheme is used for the space discretization. Various time schemes including first order implicit Euler scheme, unbounded second order backward scheme and second order Crank-Nicholson scheme have been examined in the simulations, and they give converged results in the studied problem. Therefore, Euler scheme is chosen for all simulations to reduce computational cost. The stability of the iterative algorithm is guaranteed by ensuring the Courant number to be less than 0.9 throughout the whole computational domain. Additionally, all simulations are run on NTNU supercomputer VILJE nodes (Intel Xeon E5-2670), using 2 nodes (32 cores) per simulation.

The overset grid method is employed in this work to handle the large motions of pitching foil. In the overset grid method, two separate grids are defined, which may arbitrarily overlay each other: an earth-fixed grid is used as background mesh, while a body-fitted (i.e. fitted to the foil shape) and body-fixed (i.e. fixed to the foil and moving rigidly with it) grid is used near the flapping foil (see Fig. 3, defining also the cells for information exchange between the grids). The latter is named as overset grid. The internally static grids can retain their original structure and quality but can move relative to each other without restrictions. In order to pass information between the different grids, interpolation must be performed. This method can be divided into the following four sequential steps, to be performed at every time step in dynamic simulations:

1) Identification of hole cells. They belong to the background mesh and are inside the moving body. These cells are marked and blanked out during the simulation process.

2) Identification of fringe cells. They are used as boundary cells in the calculation procedure, with boundary values determined through solution interpolation. In the background grid, these cells are adjacent to hole cells and, in the body-fitted grid, they are at the outer boundary.

3) Identification of donor cells. They are cells providing information for the fringe cells of the other mesh sufficiently close to them.

4) Interpolation between fringe and donor cells.

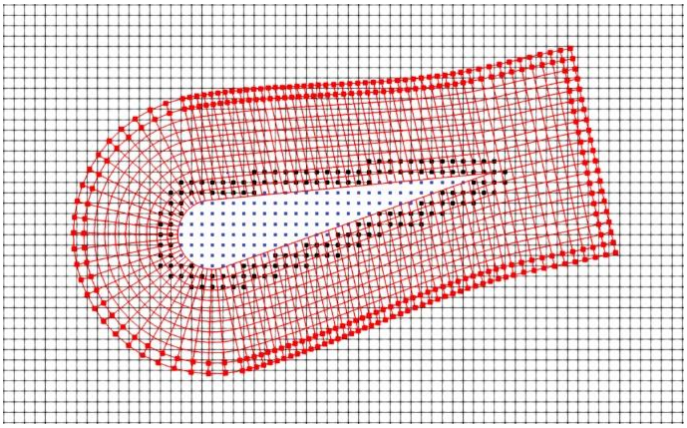

FIGURE 3: ILLUSTRATION OF OVERSET GRID METHOD. BLACK LINE: BACKGROUND MESH; RED LINE: BODY-FITTED MESH; BLUE POINTS: HOLE CELLS; BLACK AND RED POINTS: FRINGE CELLS. THE OVERSET-GRID DONOR CELLS ARE THOSE NEAR THE BLACK POINTS AND THE BACKGROUND-GRID DONOR CELLS ARE THOSE NEAR THE RED POINTS

The computational domain around the flapping foil is defined by a rectangle extending 5 chords upstream and 6.5 chords downstream. The domain height (y) is set to $-3.25c < y < 3.25c$, which is the same as the tunnel width in experiments. Numerical simulations illustrated that such dimensions are sufficient to ignore boundary effects and give converged results. Boundary conditions for this hydrodynamic problem are shown in Fig. 4. A no-slip condition is enforced along the flapping foil. Slip conditions are applied to the top and bottom domain boundaries, i.e. only velocity in y direction is enforced to be zero. A uniform inflow condition with a ramp function starting from zero to a desired constant velocity is used at the inlet while a uniform pressure condition at the outlet. The boundary conditions in the third direction for all variables are set to be empty as none of them are solved consistently with the two-dimensional (2D) flow assumption. For the interpolation layer in the overset mesh, an "overset" boundary condition is provided.

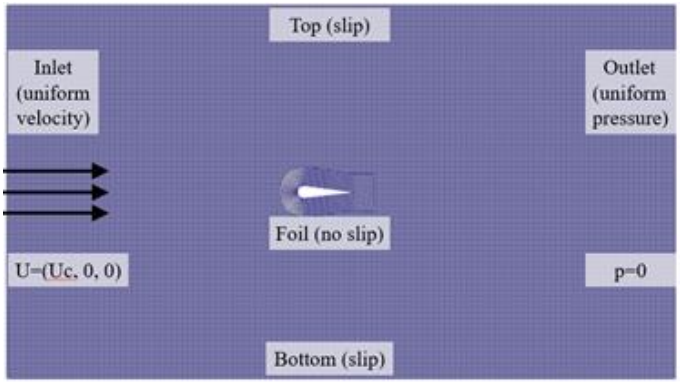

FIGURE 4: COMPUTATIONAL DOMAIN AND BOUNDARY CONDITIONS FOR THE FLAPPING FOIL

The two-dimensional grid used to discretize the flow domain close to the flapping foil (overset grid) is generated by means of the commercial software ICEM and the far away region (background grid) by means of the corresponding library included in the OpenFOAM platform. Due to the linear interpolation between grids, the overset mesh is constructed so that the outermost layer of the moving mesh has the same cell size as the background (BG) grid. Performing 2D simulations in OpenFOAM implies that the 2D grid is extruded one single cell thick in the third direction (z-axis in this work) and fluid properties are not solved in this dimension.

To confirm the spatial and temporal convergence, extensive validations on grid resolutions with the corresponding boundary conditions have been performed. The structured hexahedral cells included in three different generated grids are shown in the table below:

TABLE 1: GRID RESOLUTION FOR THE FLAPPING FOIL

	Grid 1	Grid 2	Grid 3
Nodes along foil	120	142	164
Cells in BG grid	162,000	288,000	450,000

The horizontal force coefficient, defined by the following equation:

$$C_x = \frac{\mathrm{F}_x}{\frac{1}{2}\rho U^2 c} \tag{2}$$

is used to check the numerical convergence. Here ρ is the density of the fluid. Based on this definition, the foil experiences thrust when $C_x < 0$ and drag when $C_x > 0$.

Denoting with T the foil oscillation period, the time-averaged horizontal force and force coefficient are defined as:

$$\overline{F_x} = \frac{1}{\mathrm{T}}\int_0^T F_x(t)dt \tag{3}$$

$$\overline{C_x} = \frac{1}{\mathrm{T}}\int_0^T C_x(t)dt \tag{4}$$

Fig. 5 shows the time-dependent horizontal coefficient for the flapping foil at $Re_c = 1173$, $A_D = 1.77$ and $Sr = 0.22$ (herein named as basis case) obtained with the three discretizations. Besides, the corresponding flow structures are also carefully studied. The results obtained by the examined grid sizes agree well with each other except for slight differences between the results from grid 1 and those from the other grids around minimum values. The time-averaged horizontal force coefficients and the dimensionless time-averaged streamwise velocity (u/U) along the wake centerline at $x/D = 6$ from the three discretizations are documented in Table 2. Based on these results, as compromise between local accuracy and efficiency, grid 2 is employed for all the simulations discussed in the present study.

TABLE 2: TIME-AVERAGED HORIZONTAL FORCE COEFFICIENTS AND TIME-AVERAGED VELOCITY ALONG WAKE CENTERLINE FOR THE FLAPPING FOIL

	Grid 1	Grid 2	Grid 3
$\overline{C_x}$	-0.182	-0.172	-0.164
u/U at $x/D = 6$	1.878	1.967	1.968

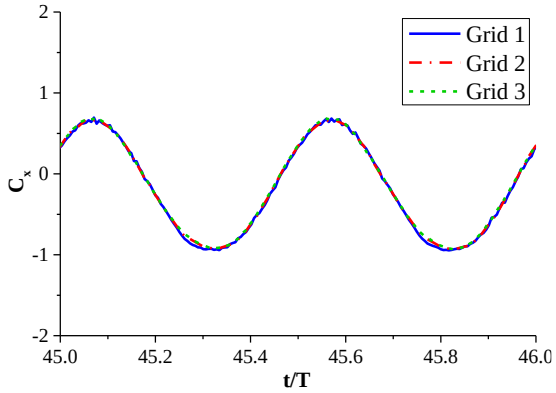

FIGURE 5: HORIZONTAL FORCE COEFFICIENT VS. TIME FOR THREE DIFFERENT GRID RESOLUTIONS. POSITIVE AND NEGATIVE VALUES INDICATE THAT THE NET FORCE IS OF DRAG- AND THRUST-TYPE, RESPECTIVELY

In addition, the basis case has been used to assess the dependence of the numerical results on the foil-fitted overset domain size. The distance from foil body to the overset boundary is set to three different values: $0.2c$ (small region), $0.33c$ (medium region) and $0.72c$ (large region). The elements number and size within the background grid are the same in these cases. The time histories of the horizontal force coefficient for the flapping foil from the three simulations are shown in Fig. 6. It is found that the computed results in the small region case are not as smooth as the other two cases, but the mean values agree well. Following these numerical tests, the medium size of overset region is applied for the rest of simulations in this work after the cost-benefit analysis. More convergence tests with respect to the overset mesh are reported in Siddiqui et al. [13].

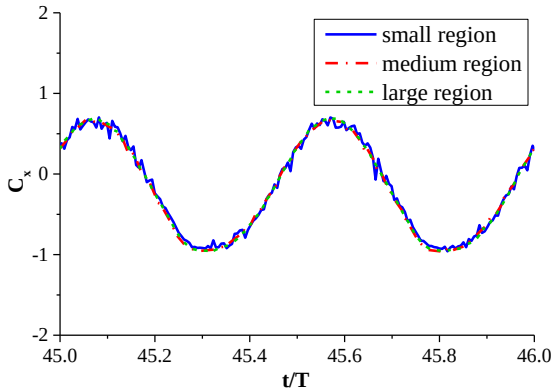

FIGURE 6: HORIZONTAL FORCE COEFFICIENTS VS. TIME FOR THREE OVERSET DOMAIN SIZES

3. RESULTS AND DISCUSSION

Based on the studies performed in the previous section, a series of cases have been simulated with varying flapping amplitude and Strouhal number to characterize the vorticity regimes in the foil-generated wake at different Reynolds numbers. Visualizations of instantaneous spanwise vorticity fields and mean flow near the foil at $Re_c = 1173$ and $Sr = 0.22$ are provided in experimental work of Godoy-Diana et al. [7], documenting mainly two-dimensional flow in the main wake of the foil at this Reynolds number. The corresponding simulation results are shown and compared with experiments in Fig. 7 and Fig. 8, respectively. The predicted flow features by the adopted method agree satisfactorily with results from the experiments.

From these comparisons, it is found that by increasing the pitching amplitude, the vK vortex street gives way firstly to a scenario where vortices of alternating signs align on the symmetry line of the wake (aligned wake), then transforms into a reverse-vK wake. Accordingly, the mean horizontal velocity behind the foil is lower than U at the smallest A_D but increases with A_D and becomes higher than U at the largest A_D, leading to a jet-flow profile. From the numerical results, the mean horizontal velocity increases practically linearly with A_D.

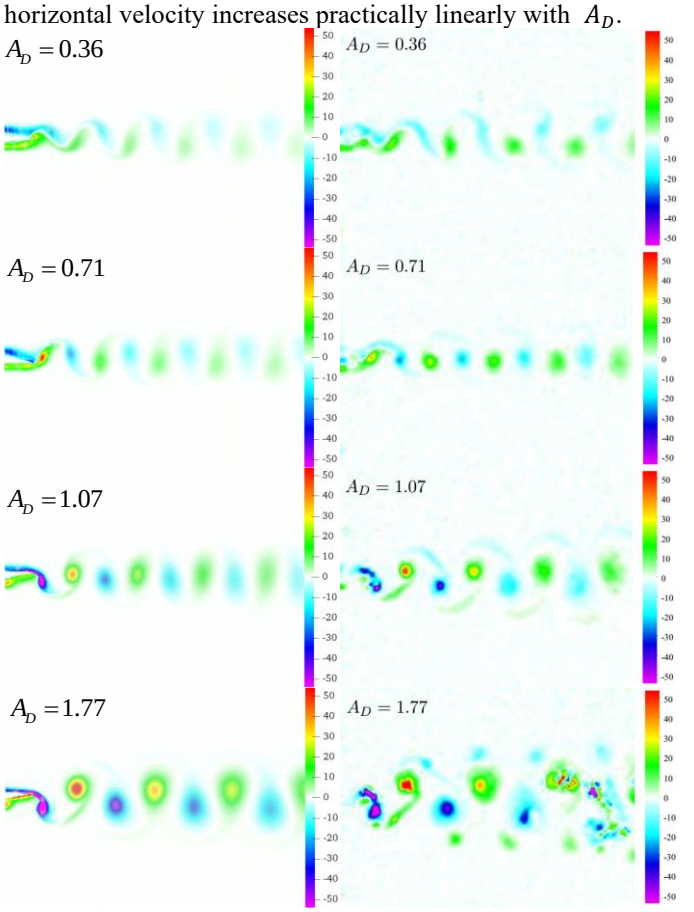

FIGURE 7: $Sr = 0.22$. FROM TOP TO BOTTOM: A_D=0.36, 0.71, 1.07, 1.77. INSTANTANEOUS SPANWISE VORTICITY FIELDS AT t=20.6s FROM OPENFOAM SIMULATIONS (LEFT) AND EXPERIMENTS [7] (RIGHT)

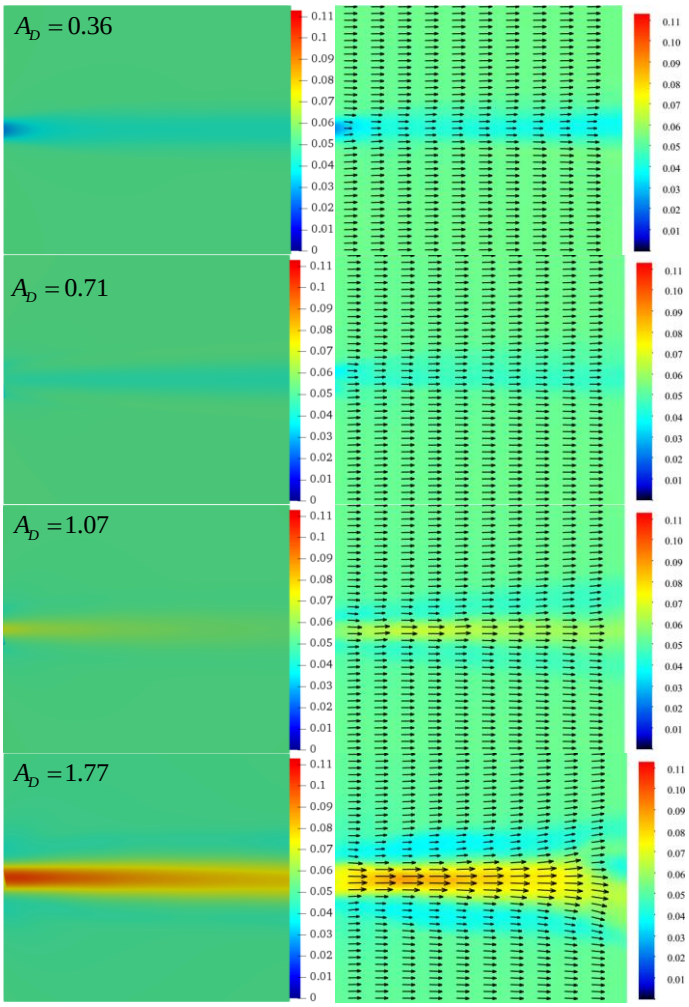

FIGURE 8: $Sr = 0.22$. FROM TOP TO BOTTOM: A_D=0.36, 0.71, 1.07, 1.77. TIME-AVERAGED FLOW VELOCITY FROM OPENFOAM SIMULATIONS (LEFT) AND EXPERIMENTS [7] (RIGHT)

All the numerical cases at different Strouhal numbers and different flapping amplitudes can form an existence diagram of the wake scenarios. The latter involve vK-type, reverse vK-type and asymmetric wake regimes. Fig. 9 shows both numerical and experimental A_D vs. Sr phase diagram, different symbols represent different types of wake. It is observed that when the flapping amplitude is fixed and the Strouhal number is varied, the transition from vK-type to reverse vK-type wake can also occur with the increase of Sr. The vK-type wake occupies primarily the lower left region of the plot but extends to higher Strouhal numbers for the lowest amplitude tested.

With increases of the Sr and A_D, the vortex structures behind the pitching foil are transited from the vK regime to the reverse-vK regime (marked by the blue line in Fig. 9), which can be univocally defined in the phase diagram when the position of vorticity maxima, at any given time and horizontal position, cross the symmetry axis of the wake. It illustrates that the transition line tends to an asymptotic value of $A_D \approx 0.6$ for $Sr > 0.4$ so that a threshold non-dimensional amplitude value exists to produce a reverse vortex street. The reverse-vK region is bounded on the other side by the transition to asymmetric regimes represented by the green line.

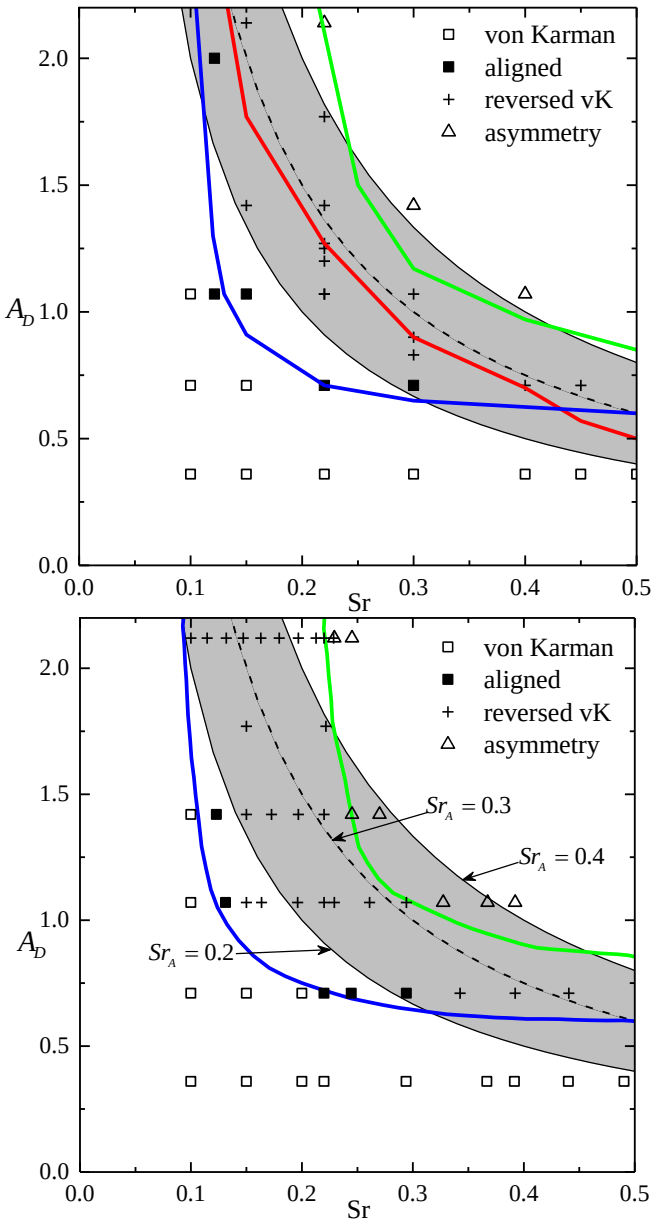

FIGURE 9: A_D VS. Sr MAP. TOP: OPENFOAM SIMULATIONS; BOTTOM: EXPERIMENTS [7]. □: VK WAKE; ■: ALIGNED VORTICES (2S WAKE); +: REVERSE VK WAKE; △: DEFLECTED REVERSE-VK STREET RESULTING IN AN ASYMMETRIC WAKE. BLUE LINE: TRANSITION BETWEEN VK-REVERSE VK. GREEN LINE: TRANSITION BETWEEN REVERSE VK AND ASYMMETRY REGIMES. RED LINE: PREDICTED CURVE WITH $C_x = 0$ WHERE THE ESTIMATED DRAG-THRUST TRANSITION OCCURS. THE GREY REGION CORRESPONDS TO THE $Sr_A = 0.3 \pm 0.1$ INTERVAL FROM THE EXPERIMENTS

In the present work, the asymmetry vortex streets behind the foil are deflected to the lower side of the symmetry line of the wake, which is opposite to the initial direction of the pitching motion, as reported by Zheng and Wei [14]. The comparison of numerical results and experimental data shows satisfactory agreement, indicating that the adopted method can be useful for further systematic parameter studies.

The mean horizontal force on the flapping foil is estimated by OpenFOAM force library based on direct integration to compare the transition from drag to thrust with that of the wake scenario. The total drag force on the foil consists of a friction drag and a form drag due to pressure distribution. The time histories of the horizontal force coefficient for the flapping foil in the four cases discussed in the previous section are shown in Fig. 10.

The values of the time-averaged horizontal force coefficients experienced by the flapping foil in the cases presented in the previous section (corresponding to $Re_c = 1173$ and $Sr = 0.22$) are documented in Table 3.

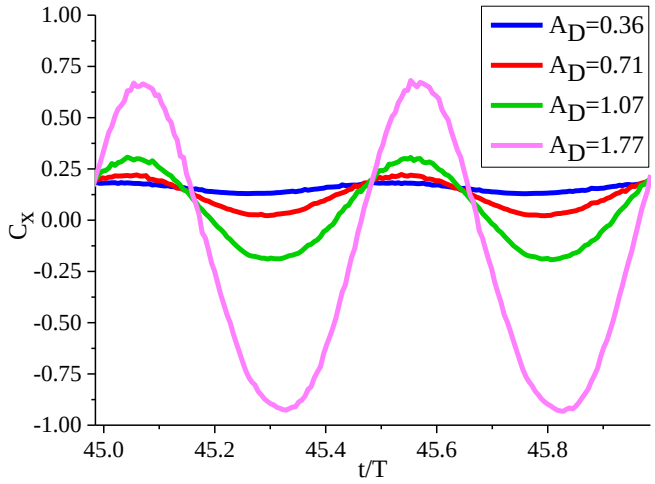

FIGURE 10: HORIZONTAL FORCE COEFFICIENT VS. TIME FOR CASES AT $Re_c = 1173$, $Sr = 0.22$, AND A_D=0.36, 0.71, 1.07, 1.77.

TABLE 3: TIME-AVERAGED HORIZONTAL FORCE COEFFICIENTS FOR THE FLAPPING FOIL

A_D	0.36	0.71	1.07	1.77
$\overline{C_x}$	0.156	0.120	0.047	-0.172

Fig. 11 shows the map of horizontal force coefficients estimated in [7] through momentum conservation equation by using experimental mean velocity fields, and the iso-contours are obtained by interpolation of measured points in Fig. 9. $\overline{C_{x0}}$, defined in [7] as the horizontal force coefficient for a non-flapping foil at zero angle of attack, is applied for normalization. Its actual value is not provided in [7] but using the corresponding predicted value from OpenFOAM leads to numerical estimates quite different from the corresponding experimental values. In order to avoid a possible error in the value of $\overline{C_{x0}}$, the following approach was used. In Fig. 11, it is found the point (0.22, 0.30) lies on the contour line $\overline{C_x}/\overline{C_{x0}} = 0.6$. Assuming that the experimental value $\overline{C_x}$ coincides with the numerical estimates, $\overline{C_{x0}}$ is estimated as $\overline{C_{x0}} = 0.266$ and this value is used to estimate $\overline{C_x}/\overline{C_{x0}}$ for all other numerical cases. As an example, Table 4 provides the predicted normalized time-averaged horizontal force coefficients for Sr= 0.22 and for A_D values. These numerical results have been included also in Fig. 11 as solid red circles labelled with their $\overline{C_x}/\overline{C_{x0}}$ value, confirming a satisfactory consistency with the experiments.

TABLE 4: PREDICTED NORMALIZED TIME-AVERAGED HORIZONTAL FORCE COEFFICIENTS AT Sr=0.22

A_D	0.36	0.71	1.07	1.77
$\overline{C_x}/\overline{C_{x0}}$	0.578	0.444	0.175	-0.638

From the results of amplitude $A_D = 0.71$ in Fig. 7, it is shown that the vortices of alternating signs align on the symmetry line of the wake, but the force calculation reveals that the foil pitching at this frequency and amplitude still generates a drag force. In fact, the horizontal force turns into a thrust force at a much higher amplitude, i.e. larger than $A_D = 1.07$.

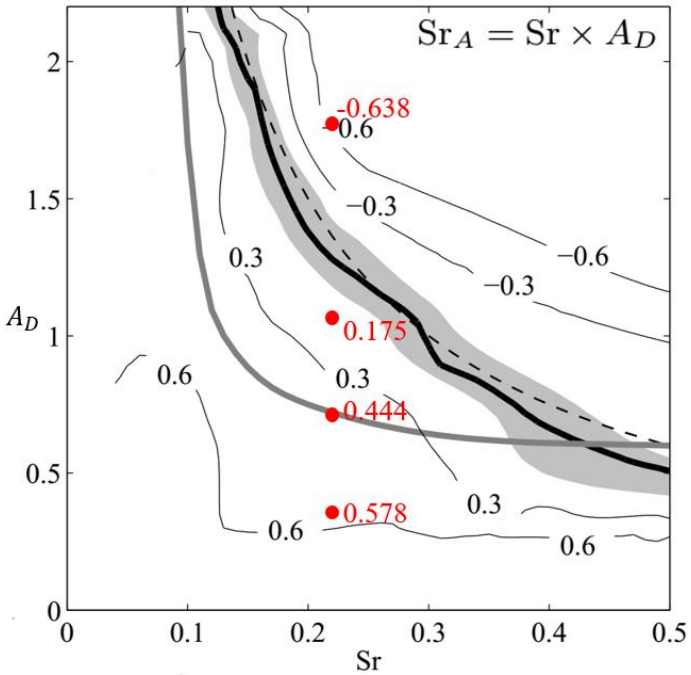

FIGURE 11: CONTOURS OF $\overline{C_x}/\overline{C_{x0}}$ ESTIMATED FROM TIME-AVERAGED VELOCITY FIELDS OF EXPERIMENTS. THE SOLID RED CIRCLES ARE NUMERICAL RESULTS, LABELLED WITH THEIR $\overline{C_x}/\overline{C_{x0}}$ VALUES

Moreover, the red line in the top of Fig. 9 marks the estimated force transition from drag to propulsive regimes for the pitching foil, which is in good agreement with the reference experimental observation. It is noted that the transition from vK to reverse-vK vorticity regime does not coincides with the drag-thrust transition. In most of the cases, the drag–thrust transition

occurs after the vK–reverse vK wake transition has occurred but before the vortices evolve into an asymmetric wake. This is not expected from inviscid-flow theory, but it agrees with many experiments.

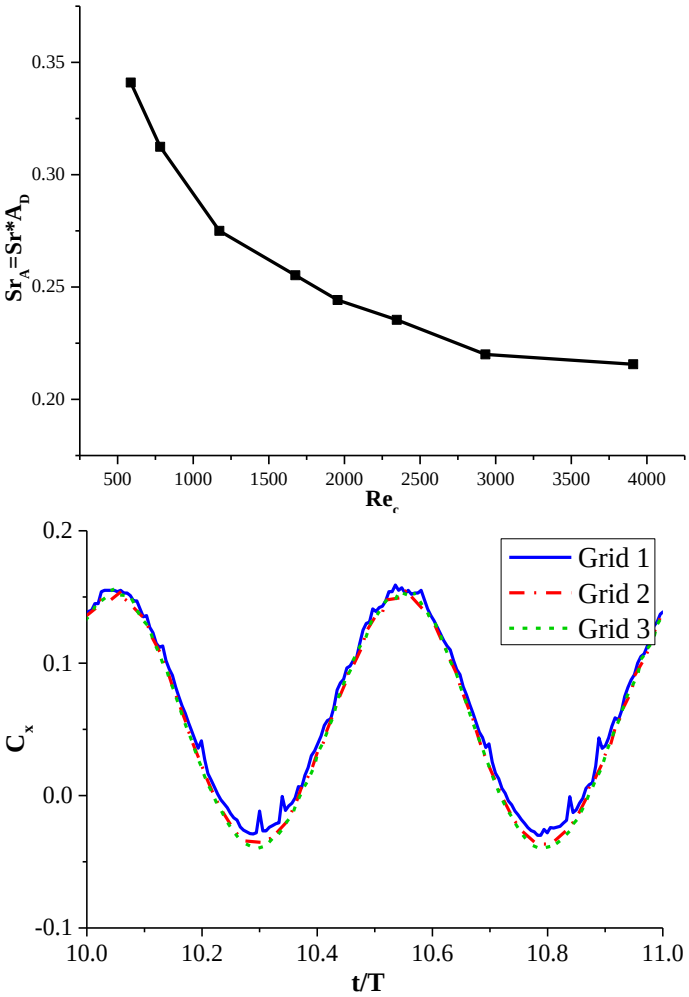

FIGURE 12: TOP: STROUHAL NUMBER VS. REYNOLDS NUMBER FOR THE PITCHING FOIL AT DRAG-THRUST TRANSITION CONDITION; BOTTOM: HORIZONTAL FORCE COEFFICIENT VS. TIME FOR THREE DIFFERENT GRID RESOLUTIONS AT $Re_c = 3910$, $A_D = 0.71$ AND $Sr = 0.22$.

To systematically quantify the effect of governing parameters on the forces and associated flow patterns of the flapping foil, numerical simulations are carried out for various Re_c and $Sr_A = Sr \times A_D$. In the present work, the kinematic viscosity of fluid is varied to ensure that only one parameter, Re_c, is changed during the study and therefore, form a clear relationship between Strouhal number and Reynolds number. Viscous-flow simulations, without turbulence model, have been performed from $Re_c = 500$ to about 4000, and the Sr_A is increased systematically from 0.1 in small increments until the time-averaged net force acting on the foil crosses zero and becomes negative. The time-dependent horizontal coefficients for the flapping foil at $Re_c = 3910$, $A_D = 0.71$ and $Sr = 0.22$ obtained with the three grid resolutions in Fig. 12 confirm the results are converged in the 2D simulations.

In general, the hydrodynamic flow features and forces on the foil at different Re_c have the same trends as those shown in Fig. 9 except that the lower left region of the phase diagram with $0 < Sr < 0.1$ in some cases contains other types of wakes, for example more than two vortices could be shed from the foil per oscillation period.

The critical Strouhal number $Sr_A{}^*$ at which the net horizontal force changes sign is not universal but depends on Re_c, as shown in Fig. 12. This confirms that the hydrodynamic forces acting on the pitching foil have strong dependence on the chord-based Reynolds number Re_c. It is found from the figure that at the drag-thrust transition curve, the amplitude-based Strouhal number $Sr_A{}^*$ is inversely related to Re_c in the present simulations. This finding is consistent with fish swimming studies by Borazjani et al. [11] and those on undulatory swimmers in nature reported by Lauder et al. [15], documenting that the swimming Sr_A increases with decreasing swimming speed (i.e. decreasing the Reynolds number). It reveals that the drag-thrust transition of the foil pitching at the forced oscillations would become closer to the vk-reverse vK wake transition curve for increasing Re_c. As the thickness-based Reynolds number $Re_D = UD/\upsilon$ is proportional to Re_c, it also indicates that the drag-thrust transition curve is strongly linked to the foil thickness-based Reynolds number Re_D.

As last note, as the Reynolds number increases, the curves for the vK-to-reverse-vK wake transition and for the drag-thrust transition get closer and the $Sr_A{}^*$ tends to be less affected by Re_c. This would suggest that at sufficiently large Reynolds number the inviscid theory can provide reliable results for the drag-thrust transition and that, therefore, rotational-flow effects dominate on viscous-flow effects. However, at this stage we cannot make a strong statement on these aspects. The next research step will then examine the role of turbulent-flow effects in this context.

4. CONCLUSION

The present work simulated the viscous flow past a flapping foil using a Navier-Stokes open-source solver. Overset grid method was employed to adapt to large amplitude motions without grid distortions. Convergence tests have been carried out to assess the dependence on grid resolution and overset domain size. The transitions in the types of wake are consistent with the benchmark experimental data, which demonstrates the efficiency and accuracy of the numerical approach. The drag-thrust transition of the pitching foil does not coincide with vK -reverse vK wake transition, indicating that more attention should be paid in this discrepancy region to ensure the gain of propulsive forces. By varying the fluid kinematic viscosity, the simulation results predict that the drag-thrust force transition depends strongly on the Reynolds number and amplitude-based Strouhal number has an inverse relationship to Re. This work provides a series of accurate numerical representations of complex flow phenomena associated with flapping foils, and it is helpful for studying the

swimming behavior of aquatic animals and guiding the design of bio-inspired underwater robots.

ACKNOWLEDGEMENTS

This work has been carried out at the Centre for Autonomous Marine Operations and Systems (NTNU AMOS) and supported by the Research Council of Norway through the Centre of Excellence funding scheme, Project number 223254-AMOS. The simulations were performed on resources provided by UNINETT Sigma2 - the National Infrastructure for High Performance Computing and Data Storage in Norway.

REFERENCES

[1] Anderson, J. M., Streitlien, K., Barrett, D. S., & Triantafyllou, M. S. (1998). Oscillating foils of high propulsive efficiency. Journal of Fluid Mechanics, 360, 41-72.

[2] Eloy, C. (2012). Optimal Strouhal number for swimming animals. Journal of Fluids and Structures, 30, 205-218.

[3] Fish, F., & Lauder, G. V. (2006). Passive and active flow control by swimming fishes and mammals. Annu. Rev. Fluid Mech., 38, 193-224.

[4] Triantafyllou, M. S., Techet, A. H., & Hover, F. S. (2004). Review of experimental work in biomimetic foils. IEEE Journal of Oceanic Engineering, 29(3), 585-594.

[5] Schnipper, T., Tophøj, L., Andersen, A., & Bohr, T. (2010). Japanese fan flow. Physics of Fluids, 22(9), 091102.

[6] Koochesfahani, M. M. (1989). Vortical patterns in the wake of an oscillating airfoil. AIAA journal, 27(9), 1200-1205.

[7] Godoy-Diana, R., Aider, J. L., & Wesfreid, J. E. (2008). Transitions in the wake of a flapping foil. Physical Review E, 77(1), 016308.

[8] Triantafyllou, M. S., Triantafyllou, G. S., & Yue, D. K. P. (2000). Hydrodynamics of fishlike swimming. Annual review of fluid mechanics, 32(1), 33-53.

[9] Müller, U. K., van den Boogaart, J. G., & van Leeuwen, J. L. (2008). Flow patterns of larval fish: undulatory swimming in the intermediate flow regime. Journal of Experimental Biology, 211(2), 196-205.

[10] Schnipper, T., Andersen, A., & Bohr, T. (2009). Vortex wakes of a flapping foil. Journal of Fluid Mechanics, 633, 411.

[11] Borazjani, I., & Sotiropoulos, F. (2008). Numerical investigation of the hydrodynamics of carangiform swimming in the transitional and inertial flow regimes. Journal of experimental biology, 211(10), 1541-1558.

[12] Chao, L. M., Pan, G., Zhang, D., & Yan, G. X. (2019). On the drag–thrust transition of a pitching foil. Ocean Engineering, 192, 106564.

[13] Siddiqui, M. A., Xu, H. L., Greco, M., & Colicchio, G. (2020). Analysis of Open-Source CFD Tools for Simulating Complex Hydrodynamic Problems. In ASME 2020 39th International Conference on Ocean, Offshore and Arctic Engineering. American Society of Mechanical Engineers Digital Collection.

[14] Zheng, Z. C., & Wei, Z. (2012). Study of mechanisms and factors that influence the formation of vortical wake of a heaving airfoil. Physics of Fluids, 24(10), 103601.

[15] Lauder, G. V., & Tytell, E. D. (2005). Hydrodynamics of undulatory propulsion. Fish physiology, 23, 425-468.